Lattice Distortions, Magnetoresistance and Hopping Conductivity in LaMnO3+δ

Article *in* Journal of Physics: Condensed Matter · December 2004

DOI: 10.1088/0953-8984/17/1/011

CITATIONS
24

READS
186

8 authors, including:

Konstantin Lisunov

119 PUBLICATIONS **1,131** CITATIONS

SEE PROFILE

V. S. Zakhvalinskiĭ

Belgorod State University

155 PUBLICATIONS **1,075** CITATIONS

SEE PROFILE

Philippe Colomban

Sorbonne Université

904 PUBLICATIONS **21,844** CITATIONS

SEE PROFILE

INSTITUTE OF PHYSICS PUBLISHING JOURNAL OF PHYSICS: CONDENSED MATTER

J. Phys.: Condens. Matter **17** (2005) 105–118 doi:10.1088/0953-8984/17/1/011

Lattice distortions, magnetoresistance and hopping conductivity in $LaMnO_{3+\delta}$

R Laiho[1], K G Lisunov[1,2], E Lähderanta[1,3], V S Stamov[1,2], V S Zakhvalinskii[1,4], Ph Colomban[5], P A Petrenko[2] and Yu P Stepanov[6]

[1] Wihuri Physical Laboratory, University of Turku, FIN-20014 Turku, Finland
[2] Institute of Applied Physics, Academiei Street 5, MD-2028 Kishinev, Moldova
[3] Department of Physics, Lappeenranta University of Technology, PO Box 20, FIN-53851, Lappeenranta, Finland
[4] Belgorod State University, Pobeda Street 85, 308015 Belgorod, Russia
[5] LADIR UMR 7075 CNRS and University Pierre and Marie Curie, France
[6] A F Ioffe Physico-Technical Institute, 194021 St Petersburg, Russia

Received 13 May 2004, in final form 21 October 2004
Published 10 December 2004
Online at stacks.iop.org/JPhysCM/17/105

Abstract

Structural and transport properties of ceramic $LaMnO_{3+\delta}$ are investigated for $\delta = 0$–0.154. According to x-ray diffraction measurements at room temperature the crystal structure of this compound varies from orthorhombic ($Pbnm$) for $\delta = 0$ to rhombohedrally distorted cubic ($Pm3m$) for $\delta = 0.065$–0.112 and to rhombohedral ($R\bar{3}c$) crystal symmetry for $\delta = 0.125$–0.154. These structural modifications are confirmed by the Raman micro-spectroscopy measurements. The resistivity displays in the range $\delta = 0$–0.154 an activated behaviour both above and below the paramagnetic (PM) to ferromagnetic transition temperature, T_C. In the field of 8 T the relative magnetoresistance, $\Delta\rho(B)/\rho(0)$, reaches at $\delta = 0.154$ the values of -88% near T_C and -98% at $T \approx 20$ K. The resistivity of the PM phase of $LaMnO_{3+\delta}$ with $\delta = 0.100$–0.154 satisfies the Shklovskii–Efros-like variable-range hopping (VRH) conductivity law between $T_C \sim 130$–160 K and the VRH onset temperature $T_v \sim 250$–270 K. The resistivity is governed by a complex energy dependence of the density of the localized states near the Fermi level, comprising a soft Coulomb gap $\Delta \approx 0.43$–0.48 eV and a rigid gap $\gamma \approx 0.14$–0.17 eV, the latter being connected to formation of small polarons.

(Some figures in this article are in colour only in the electronic version)

1. Introduction

$LaMnO_{3+\delta}$ belongs to the hole-doped mixed-valence perovskites, which have attracted much attention due to the colossal magnetoresistance (CMR) effect accompanied by a metal–insulator transition (MIT) [1–3]. These compounds have a rich magnetic phase diagram, exhibiting the high-temperature paramagnetic (PM), the ferromagnetic (FM) and the canted

antiferromagnetic spin orderings [2, 3], as well as spin-glass or cluster-glass behaviour [4, 5]. The electronic properties of the manganite perovskites are governed by competing Mn^{3+}–Mn^{3+} superexchange and Mn^{3+}–Mn^{4+} double-exchange interactions, by local Jahn–Teller distortions and by charge ordering and phase separation effects [2, 3].

In various CMR compounds adiabatic nearest-neighbour hopping (NNH) conductivity of small polarons satisfying the Arrhenius law is observed above room temperature [2, 3]. In $La_{1-x}Ca_xMnO_3$ this behaviour persists up to $T \sim 700$ K [6] and 1200 K [7]. Below room temperature the hopping conductivity is strongly influenced by features of the density $g(\varepsilon)$ of the localized states (DOS) near the Fermi level, μ [8]. As shown by scanning tunnelling spectroscopy of a $La_{0.8}Ca_{0.2}MnO_3$ film the structure of the DOS is complex around μ, including a parabolic interval with width $\Delta \sim 0.4$ eV (the soft gap) and a region of $g(\varepsilon) = 0$ with width $\gamma(T)$ up to ~0.11 eV (the rigid gap) [9]. The soft gap is attributed to Coulomb interactions (and referred to as the *Coulomb gap* [10]) between localized charge carriers. The rigid gap is associated with the Jahn–Teller effect [9]. Generally, on lowering the temperature it is energetically favourable for charge carriers to hop beyond the nearest-neighbour sites, leading to variable-range hopping (VRH) conductivity [11]. The Mott VRH conductivity would set in when the DOS around μ is finite and constant [11], whereas the soft Coulomb gap leads to another type of deviation from the Arrhenius law, the Shklovskii–Efros (SE) VRH conductivity [10]. In turn, the rigid gap modifies the SE-VRH conductivity law [8]. Detailed analysis of the resistivity [8] and the thermopower [12] in $La_{0.7}Ca_{0.3}Mn_{1-y}Fe_yO_3$ above T_C has allowed us to establish the value of $\Delta \approx 0.4$ eV and $\gamma(T) \approx \gamma(T_v)\ (T/T_v)^{1/2}$ with the onset of the SE-VRH conductivity at $T_v \approx 310$–330 K and $\gamma(T_v) = 0.12$–0.16 eV (decreasing with y) supporting the results in [9].

Until now the electronic properties of $LaMnO_{3+\delta}$ have been investigated much less than e.g. for its close analogue $La_{1-x}Ca_xMnO_3$. On the other hand, because both materials are obtained by hole doping from the same parent compound, $LaMnO_3$, the electronic properties of non-stoichiometric $LaMnO_{3+\delta}$ are expected to be no less interesting than those of $La_{1-x}Ca_xMnO_3$ [2, 3]. Basically, the difference between $La_{1-x}Ca_xMnO_3$ (or $La_{1-x}Ca_xMn_{1-y}Fe_yO_3$) and $LaMnO_{3+\delta}$ lies in the methods of hole doping, the substitution of Ca^{2+} for La^{3+} in the former case and creation of lattice defects in the latter. Instead of excess oxygen, which cannot occupy interstitial sites of the perovskite structure [13], the non-stoichiometry of $LaMnO_{3+\delta}$ is connected to cation vacancies with the concentration of $\delta' = (2/3)\delta$, corresponding to the relative hole concentration (or the value of the ratio Mn^{4+}/Mn^{3+}) $c = 2\delta$. The absence of Ca atoms leads to a reduced lattice disorder and more homogeneous hole distribution in $LaMnO_{3+\delta}$ than in $La_{1-x}Ca_xMnO_3$, as follows from the differences between these compounds in the values of the magnetic irreversibility, in the dependences of the low-field magnetic susceptibility, χ, and the PM to FM transition temperature, T_C, on c or δ and in the critical behaviour of $\chi(T)$ near T_C [14].

In this paper we investigate the Raman scattering and magnetoresistance as a function of δ in $LaMnO_{3+\delta}$. The Raman spectra are related to distortions of the MnO_6 octahedra and evolution of the short-range order with stoichiometry. Measurements of the resistivity and the magnetoresistance provide important microscopic information about the conductivity mechanisms and the energy spectrum of the charge carriers, including details of the DOS around the Fermi level.

2. Sample preparation and characterization

Ceramic $LaMnO_{3+\delta}$ samples were prepared with a three-stage process. In the first stage the standard solid-state reaction, similar to that for $La_{1-x}Ca_xMnO_3$ [4, 15], by mixing La_2O_3 and

MnO_2 and heating in air at 1320 °C for 40 h with intermediate grindings, was used. Then the obtained powder was pressed into pellets under the pressure of 2000 kg cm^{-2} and annealed in air at 1370 °C for 22 h. According to x-ray diffraction data the samples had a cubic structure with the lattice parameter $a = 7.813(2)$ Å modified by a small rhombohedral distortion. The same value of $\delta \approx 0.065$ was obtained by the gravimetric and iodine titration methods [14], showing that these samples were of the non-stoichiometric $LaMnO_{3+\delta}$ form.

In the second stage the prepared material was subjected to long annealing in flowing Ar [13] to obtain the stoichiometric $LaMnO_{3.00}$ composition. In the third stage a set of $LaMnO_{3+\delta}$ samples with $\delta = 0, 0.065, 0.100, 0.112, 0.125, 0.133, 0.140$ and 0.154 (denoted below as S000, S065, . . ., S154) was prepared by combining Ar and oxygen treatments and annealing in air using different temperatures and annealing times (for details see [14]).

According to the room temperature x-ray diffraction investigations our $LaMnO_{3+\delta}$ samples fall into three groups:

(i) S000 with orthorhombic $Pbnm$ structure and lattice parameters $a = 5.531(1)$ Å, $b = 5.536(1)$ Å and $c = 7.689(2)$ Å,
(ii) S065, S100 and S112 having cubic $Pm3m$ structure with small rhombohedral distortions and the lattice parameter decreasing with δ between $a = 7.813(2)$–$7.791(1)$ Å and
(iii) S125, S133, S140 and S154 with the rhombohedral $R\bar{3}c$ structure and the lattice parameters decreasing with δ in the intervals of $a = 5.530(2)$–$5.516(1)$ Å and $c = 13.333(5)$–$13.311(4)$ Å.

In terms of the cation vacancies, V^{La} and V^{Mn}, $LaMnO_{3+\delta}$ can be expressed in a form equivalent to $La_{1-\varepsilon}Mn_{1-\varepsilon}O_3$ with $\varepsilon = \delta/(3+\delta)$ [13] as

$$LaMn^{3+}_{1-2\delta}Mn^{4+}_{2\delta}O_{3+\delta} = \frac{3+\delta}{3}La_{3/(3+\delta)}V^{La}_{\delta/(3+\delta)}Mn^{3+}_{(3-6\delta)/(3+\delta)}Mn^{4+}_{6\delta/(3+\delta)}V^{Mn}_{\delta/(3+\delta)}O_{3.00}. \quad (1)$$

In $ABO_{3+\delta}$ perovskite oxides the oxygen is located on sites equivalent to the oxygen anions [13, 16]. Actually we found that δ is changed in $LaMnO_{3+\delta}$ during treatment in flowing Ar or O_2 gas or in open air at a high temperature. Under this treatment oxygen is absorbed by reactions with La and Mn in the volume of the specimen [13, 17, 18]. As a result new unit cells and additional La and Mn defects appear, as evidenced by the growth of the size of the samples. Positive deviations of δ cannot be explained in the perovskite oxides by the presence of excess oxygen in the structure [18]. In agreement with equation (1) δ is connected to the number of La and Mn defects and the oxygen content is always stoichiometric.

3. Raman scattering

The surface and near-surface volume of samples S000, S065 and S154 was analysed using back-scattering Raman micro-spectroscopy at the magnifications of 500× or 1000×. The 458, 532, 514.5, 633 and 647 nm wavelengths were used as excitation sources. The spectrometers were

(i) a notch filtered Infinity spectrograph with resolution 2 cm^{-1} (Dilor, Lille, France) equipped with a Peltier cooled CCD, the exciting power ranging between 0.01 and 0.1 mW, and
(ii) an XY (Dilor) spectrograph with resolution 1 cm^{-1}, equipped with a liquid nitrogen cooled CCD matrix (2000 × 256 pixels).

The exciting power was 0.1–1 mW on the sample. In order to control the sample homogeneity and the polarization effect, single grains were selected for the measurements and the spectra were recorded automatically using the Labspec 2.0 software (Dilor) and decomposed using

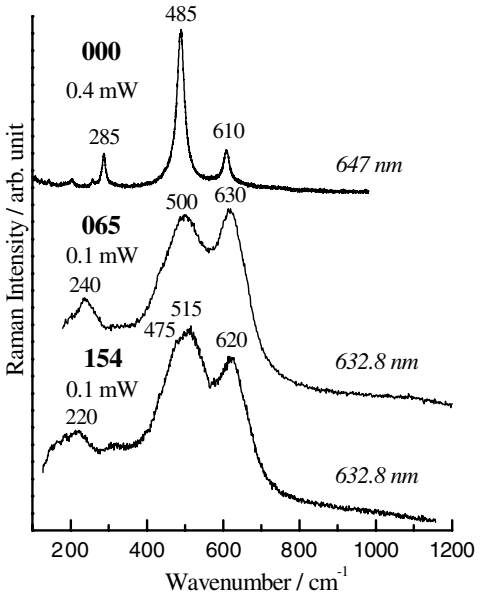

Figure 1. Raman spectra for samples S000, S065 and S154 recorded at room temperature using the given excitation wavelengths and the laser powers.

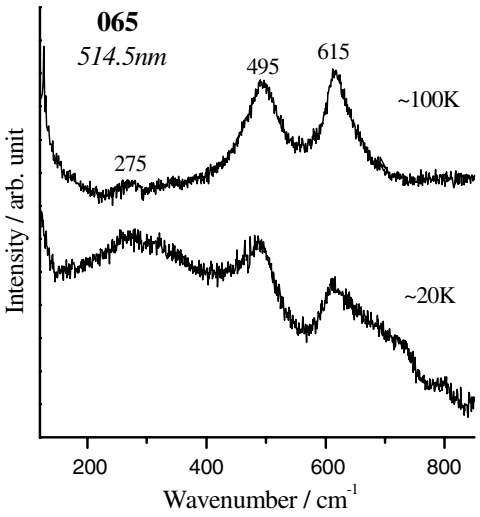

Figure 2. Raman spectra recorded on S065 at $T = 100$ and 20 K using green excitation at $\lambda = 514.5$ nm.

the Origin 5.0 software. According to the resonant or near-resonant character of the Raman spectra we choose to fit the band shape with a Lorentzian function.

In figure 1 are shown the Raman spectra recorded at room temperature for S000, S065 and S154 samples. Comparison with literature [19] confirms the orthorhombic and rhombohedral structures of S000 and S065, respectively. Change of an ordered structure (S000) to disordered ones (S065 and S154) is evident from the strong broadening of the Raman line widths. The small splitting observed in the spectrum of S154 indicates that the short-range order is, however, better than in S065. The lines at $\sim$485 and 610 cm^{-1} arise from the stretching modes of the MnO_6 octahedra [20]. If the spectra are recorded on specific ceramic grains using the high-magnification microscope objective (1000$\times$), the relative intensity of these two modes changes from grain to grain due to the strong polarization of the modes: at a first approximation only oxygen atoms move in these modes and the bandwidth is thus very sensitive to the disorder of the oxygen sublattice and any change of the Mn–O bond. We can say approximately that the changes of the electron number involved in the bonding modify the band intensity while the changes in the Mn–O distance shift the wavenumber. The superimposition of the different configurations broadens the Raman components. On the other hand the lines at $\sim$280 cm^{-1} and below are related to the bending modes and external modes and are more sensitive to the cation sublattice disorder. The great broadening of the S065 spectrum can be assigned to disorder (shift in position or vacancies of the atoms around the oxygen atoms, change of the Mn valence). The band splitting of the 515 nm line in S154 confirms the lower symmetry of this sample as observed on the x-ray powder diffraction pattern. The wavenumber shift is consistent with the variation of the unit-cell volume.

As evident from figure 2 the differences of the Raman spectra at two different temperatures confirm that the S065 sample undergoes a structural transition. The 20 K Raman spectrum shows a broad Rayleigh wing and the intensity of the 490–610 cm^{-1} doublet vanishes. The

Table 1. The wavenumbers of the main Raman components (in cm^{-1}) for S000 and S065 excited at different wavelengths λ.

λ (nm)	S000			S065		
457	283	485	607	238	495	638
532	288	488	609	235	500	623
632	286	488	609	268	498	628
647	287	488	609	247	488	628

Table 2. The wavenumbers of the main Raman components (in cm^{-1}) for S154 excited at $\lambda = 632.8$ nm.

S154
220
310
475
515
620

spectrum looks very similar to that observed in $La_{67}Ca_{33}MnO_3$ with broad overdamped low-wavenumber scattering.

In table 1 are given the wavenumbers of the main Raman components for S000 and S065 and in table 2 those for S154 under excitation with $\lambda = 632.8$ nm light.

4. Resistivity and magnetoresistance

Investigations of $\rho(T)$ were made using the four-probe technique in the transverse magnetic field configuration ($\mathbf{B} \perp \mathbf{j}$) for $B = 0$–10 T. The sample was inserted in a He exchange gas Dewar, where its temperature could be varied between 4.2 and 350 K to an accuracy of 0.5%.

As shown in figure 3 (upper panel) the resistivity decreases with increasing δ, the variation being more rapid between $\delta = 0$ and 0.065 and slowing down when δ is increased from 0.1 to 0.154. The dependence of ρ on T exhibits a weak inflection near T_C (the open triangles in figure 3 and the other figures show the data of T_C, obtained in [12] for the same samples as in the present work). This inflection is more pronounced in S100, S125 and S154 (see also the lower panel of figures 3 and 4) and disappears when B is increased, as typical of the PM–FM transition. The resistivity has an activated character for all δ (and $c = 2\delta = 0$–0.308) in the whole temperature range, without exhibiting any sign of the MIT with lowering T. This is different from $La_{1-x}Ca_xMnO_3$ which shows a steep decrease of $\rho(T)$, characteristic of MIT, with decreasing T below T_C for $c > 0.18$–0.20 [2, 3]. The additional inflections of $\rho(T)$ in S154 can be seen at $T \sim 70$ and 45 K (inset to figure 4).

The magnetoresistance (MR) of S000 is negligible, which is connected to the absence of Mn^{4+}, whereas all the hole-doped samples S065–S154 exhibit the CMR effect as evident from figures 3 and 4. Similar to bulk ceramic $La_{1-x}Ca_xMnO_3$ [1–3, 21] the relative MR defined as $\Delta\rho/\rho_0 \equiv [\rho(B) - \rho(0)]/\rho(0)$ attains a minimum of -67%, -64%, -72% and -88% at $B = 8$ T in S065, S100, S125 and S154, respectively, at a temperature T_m close to T_C (see figure 5). In addition, as shown in the inset to figure 5, T_m has a maximum at $\delta_m \approx 0.1$, coinciding with that of T_C, whereas $|\Delta\rho/\rho_0|$ attains a minimum at δ_m. Another feature in figure 5 (which does not take place in $La_{1-x}Ca_xMnO_3$) is a complicated temperature dependence of MR below T_C or T_m, consisting of a maximum at $T \sim 80$–110 K and an

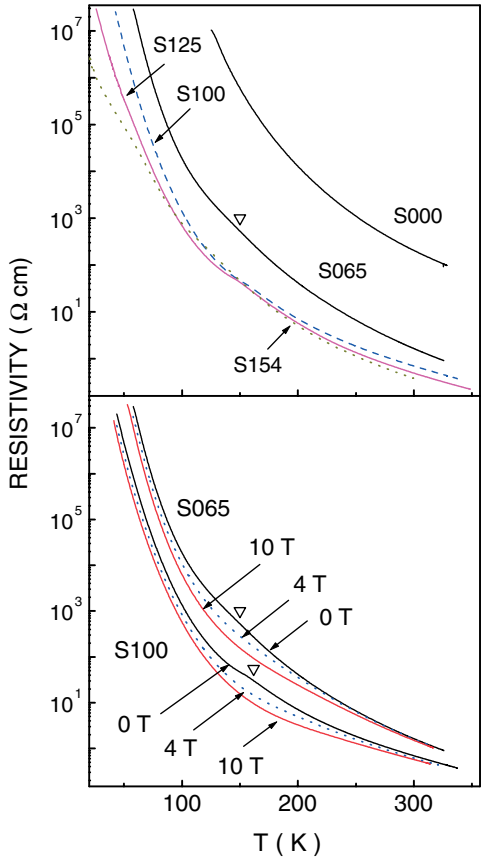

Figure 3. The temperature dependence of the resistivity for S000, S065, S100, S125 and S154. The open triangle marks T_C for S065 (upper panel). The temperature dependence of the resistivity for S065 and S100 in different magnetic fields. The open triangles mark T_C for S065 and S100 (lower panel).

additional minimum with $\Delta\rho/\rho_0 = -62\%$ at $T \approx 50$ K in S100 and -79% at $T \approx 40$ K in S125 (which is even lower than the minimum at T_m in S125). In S154 the second MR minimum is not observed and below $T \sim 100$ K the MR decreases monotonically on lowering the temperature, reaching at $T \approx 20$ K the value of $\Delta\rho/\rho_0 \approx -98\%$, more typical for optimally doped $La_{0.67}Ca_{0.33}MnO_3$ films near the MIT [2, 3, 21].

Hence, having the property of CMR near T_C common with $La_{1-x}Ca_xMnO_3$, the resistivity and MR of $LaMnO_{3+\delta}$ exhibit a set of new features, including

(i) absence of MIT at Mn^{4+}/Mn^{3+} as high as $c \approx 0.3$,
(ii) non-monotonic dependence of T_C, T_m and $\Delta\rho/\rho_0$ on the hole concentration c (more strictly, on δ connected to c) and
(iii) a complicated temperature dependence of MR below T_C.

As mentioned in the introduction, investigations of the magnetic properties of $LaMnO_{3+\delta}$ have shown that the hole distribution is more homogeneous and intrinsic lattice disorder is reduced in this compound with respect to $La_{1-x}Ca_xMnO_3$ due to absence of the Ca atoms to create the holes [14]. This is also consistent with the negligible phase separation effect,

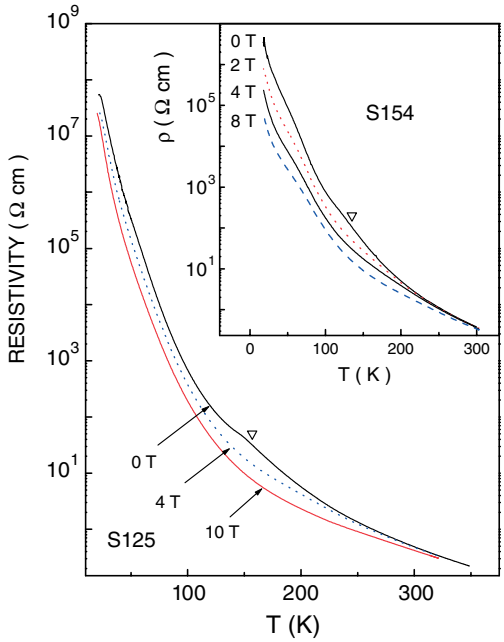

Figure 4. Temperature dependence of the resistivity of S125 and S154 (inset) in different magnetic fields. The open triangles mark T_C.

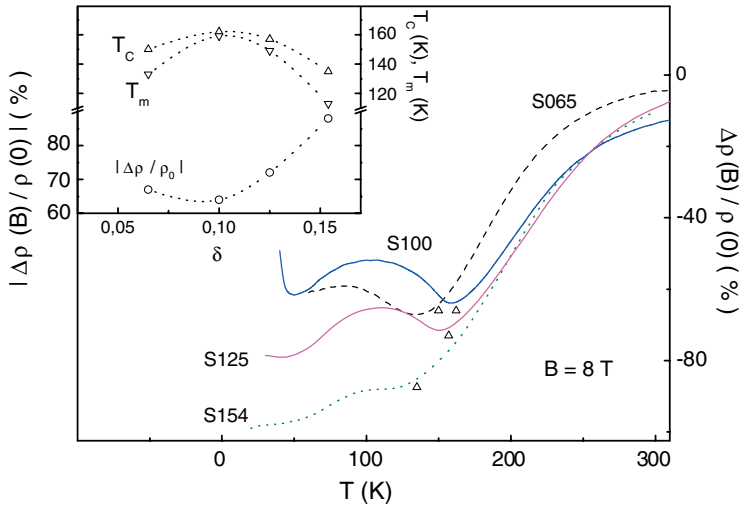

Figure 5. Temperature dependence of the relative magnetoresistance in the field of $B = 8$ T. The open triangles mark T_C. Inset: dependences of T_C, T_m and the value of the relative MR on δ.

as evident from the absence of the contribution of the hole-rich FM metallic regions in the nonmetallic PM matrix (pertinent to many CMR materials [2, 3, 22, 23]) to the critical behaviour of $\chi(T)$ near T_C [14]. Therefore, a likely reason for the absence of MIT in our $LaMnO_{3+\delta}$ samples may be attributed to a connection of MIT to the phase separation in manganite perovskites [24], although other reasons, determined even by the sample preparation details,

cannot be excluded (indeed, an interval of metallic conductivity below T_C in $LaMnO_{3+\delta}$ with δ between 0.14 and 0.18 was observed in [13]). The non-monotonic dependence of T_C (δ) has been interpreted by a competition between an increase of the hole concentration and a decrease of the bandwidth of the localized holes when δ is increased, the latter being due to increasing distortions of the perovskite cubic structure [14]. Hence, the non-monotonic dependence of CMR at $T_m \sim T_C$ may be connected to a similar reason.

The additional inflections of $\rho(T)$ in S154 and the complicated non-monotonic behaviour of the MR below T_C in all the investigated $LaMnO_{3+\delta}$ samples may result from an interplay between orderings of the spin and the orbital degrees of freedom, accompanied with some weakening of the electron–phonon coupling and, therefore, decreasing of the local distortions of the crystal lattice when T is decreased. However, unlike the inflection near T_C, the inflections of the resistivity curve in S154 below T_C do not vanish in the applied fields up to $B = 8$ T. In addition, any serious reconstruction of the spin system should be manifested in the magnetic properties of the material, whereas no qualitative difference of $\chi(T)$ is observed in $LaMnO_{3+\delta}$ [14] and $La_{1-x}Ca_xMnO_3$ [4] below T_C. This does not permit us to exclude some extrinsic reasons for the additional inflections of $\rho(T)$ in S154 and feature (iii) above, requiring probably more detailed sample characterization.

Unlike the temperature interval below T_C, the behaviour of $\rho(T)$ and MR in the PM phase of $LaMnO_{3+\delta}$ ($T > T_C$) is typical of the manganite perovskites and other CMR compounds [2, 3, 6–8], allowing a deeper analysis, which will be done in the next section.

5. Hopping conductivity

5.1. Theoretical background

Following the introduction, we analyse the resistivity of $LaMnO_{3+\delta}$ above T_C with the law

$$\rho(T) = \rho_0(T) \exp[(T_0/T)^p], \tag{2}$$

where T_0 is a characteristic temperature and $p = 1$ for NNH (in this case the activation energy $E_0 \equiv kT_0$ is usually introduced instead of T_0), $p = 1/4$ for the Mott [11] and $1/2$ for the SE-VRH regimes [10]. If a condition $\Gamma \equiv [kT(T_0/T)^p\alpha/(2\hbar s)]^2 \gg 1$ is satisfied, the prefactor is given by the equation

$$\rho_0(T) = AT^m \tag{3}$$

where

$$A = C\alpha^{11}T_0^{(7+q)p}, \tag{4}$$

α is the localization radius of the charge carriers, s is the sound velocity (equal to 6.8×10^5 cm s^{-1} in $La_{1-x}Ca_xMnO_3$ [25]) and C is a constant [8]. For the SE mechanism $m = 9/2$ or $5/2$ and for the Mott VRH conductivity $m = 25/4$ or $21/4$, if the wavefunction ψ of the localized carriers has the conventional hydrogen-like form $\psi_1(r) \sim \exp(-r/\alpha)$ (corresponding to $q = 0$ in equation (4)) or $\psi_2(r) \sim r^{-1}\exp(-r/\alpha)$ (corresponding to $q = 4$ in equation (4)), respectively. The wavefunction ψ_2 sets in when the fluctuating short-range potential connected to the lattice disorder is important to localization [10]. For the adiabatic NNH conductivity $m = 1$ for any Γ, ψ and q [10, 11]. In equation (2) $T_0 = T_{0M}$ or T_{0SE} for $p = 1/4$ or $1/2$, respectively, where

$$T_{0M} = \beta_M/[kg(\mu)\alpha^3] \qquad \text{and} \qquad T_{0SE} = \beta_{SE}e^2/(\kappa k\alpha), \tag{5}$$

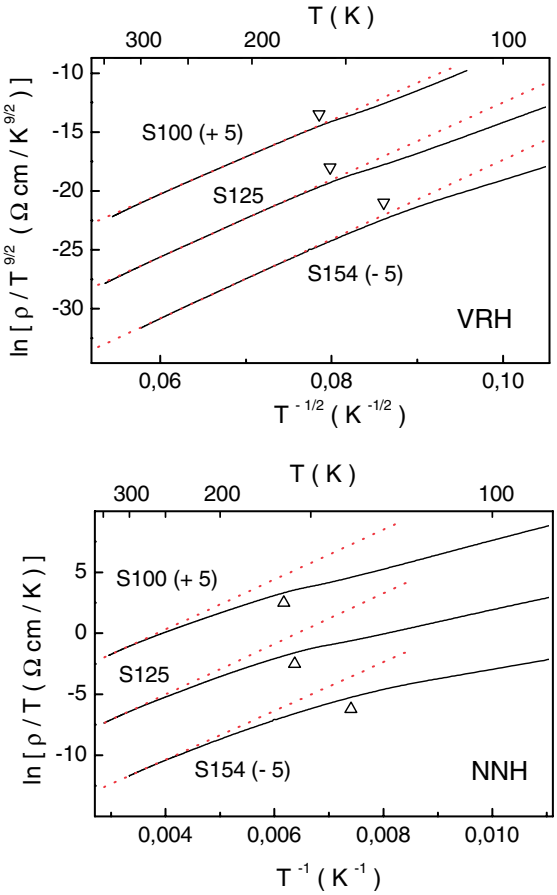

Figure 6. The dependence of $\ln(\rho/T^{9/2})$ on $T^{-1/2}$. The open triangles mark $T_C^{-1/2}$ (upper panel). The dependence of $\ln(\rho/T)$ on T^{-1}. The open triangles mark T_C^{-1} (lower panel). For convenience the plots for S100 and S154 are shifted along the y-axis by ± 5 units.

κ is the dielectric constant, $\beta_M = 21$ and $\beta_{SE} = 2.8$ [10]. Presence of the rigid gap $\gamma < \Delta$ modifies the SE-VRH by changing the characteristic temperature from T_{0SE} to T_0 [8] given by the equation

$$T_0 = \left(\frac{\gamma}{2k\sqrt{T}} + \sqrt{\frac{\gamma^2}{4k^2T} + T_{0SE}} \right)^2 . \tag{6}$$

As can be seen from equations (5), T_{0SE} and T_{0M} are independent of T for constant α or $g(\mu)\alpha^3$, respectively. From equation (6) it follows that T_0 does not depend on T if, additionally, one out of the following two conditions are satisfied, (i) $\gamma/(2kT) \ll (T_{0SE}/T)^{1/2}$ and $\gamma \sim T$ and (ii) $\gamma \sim T^{1/2}$. For (i) we have $T_0 = T_{0SE}$ because $(T_0/T)^{1/2} \approx (T_{0SE}/T)^{1/2} + \gamma/(2kT)$, and if $\gamma \sim T$ the second term is constant and can be included in the prefactor, while for (ii) one gets $T_0 \neq T_{0SE}$.

5.2. Analysis of the experimental data

As can be seen from the bottom panel of figure 6 the plots of $\ln(\rho/T)$ versus $1/T$ for samples S100, S125 and S154 display a tendency of NNH conductivity with increasing T. However, the

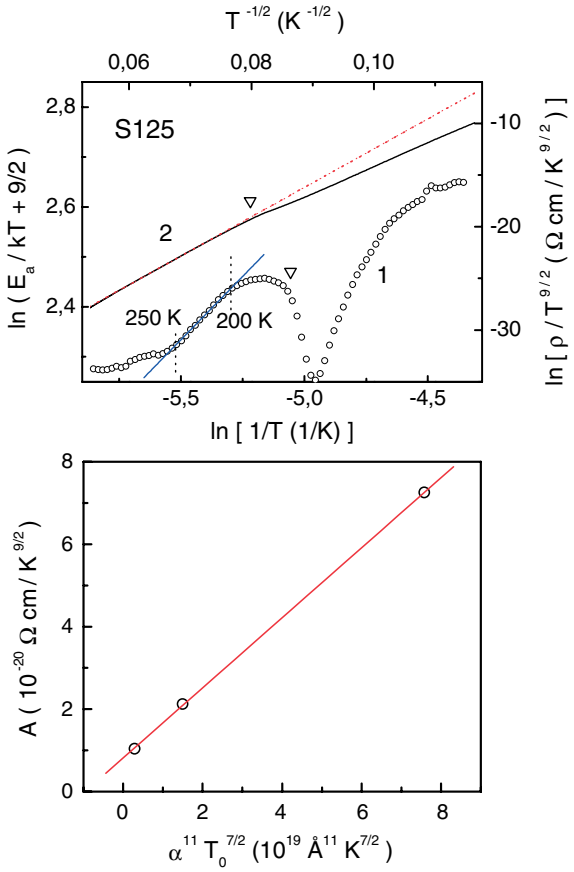

Figure 7. The plots of $\ln(E_a/kT + 9/2)$ versus $\ln(1/T)$ (plot 1, O) and $\ln(\rho/T^{9/2})$ on $T^{-1/2}$ (plot 2, full curve) for S125. The dotted line represents a linear fit. The open triangles mark $T_C^{-1/2}$ and $\ln(1/T_C)$ (upper panel). The plots of A versus $\alpha^{11}T_0^{7/2}$ (lower panel).

value of the activation energy $E_0 \approx 0.18$ eV (approximately equal for all samples) could only be found roughly due to small intervals of ΔT, where the experimental data could be fitted with equation (2) by putting $p = 1$, $T_0 = E_0/k$ and $\rho_0(T) \sim T$. On the other hand, the deviations from the NNH conductivity well above T_C suggest a transition to the VRH conductivity with lowering T. The best fit of the data with equation (2), assuming constant T_0, is obtained for $p = 1/2$ and $m = 9/2$ within a much wider temperature interval, limited by temperatures sufficiently close to T_C (the upper panel of figure 6). A correspondence of our resistivity data to the SE-VRH conductivity at $\Gamma \gg 1$ and $\psi = \psi_1$ (yielding the values of p and m above) is supported by analysis of the local activation energy, $E_a(T) \equiv \mathrm{d}\ln\rho(T)/\mathrm{d}(kT)^{-1}$ [10]. As follows from equation (2), in the temperature interval where T_0 does not depend on T, $E_a(T)$ can be expressed in the form $\ln[E_a/(kT) + m] = \ln p + p\ln T_0 + p\ln(1/T)$. As shown in the upper panel of figure 7 the plot of $\ln[E_a/(kT) + 9/2]$ versus $\ln(1/T)$ can be fitted with a linear law, giving $p = 1/2$. In addition, such plots yield the most accurate values of the onset temperature T_v (the upper limit of the SE-VRH conductivity regime), which are collected in table 3, while the values of A in equation (3) and those of T_0 are obtained by fitting of the plots

Table 3. The values of the coefficient A, the characteristic VRH temperature, T_0, the onset VRH temperature, T_v, the widths of the Coulomb gap, Δ, and the rigid gap, γ, and the localization radius α.

Sample	A (10^{-20} Ω cm $K^{-9/2}$)	T_0 (10^4 K)	T_v (K)	Δ (eV)	$\gamma(T_v)$ (eV)	α (Å)
S100	7.3	9.8	250	0.43	0.13	1.7
S125	2.1	10.8	250	0.46	0.16	1.4
S154	1.0	11.3	270	0.48	0.17	1.2

in the upper panel of figure 6 (see table 3). Using the temperature parameters, the values of the Coulomb gap were evaluated with the equation $\Delta \approx k(T_0T_v)^{1/2}$ [8] and are displayed in table 3.

The existence of the temperature interval where T_0 is constant, as evident from the upper panels of figures 6 and 7, suggests that one of the cases mentioned in the comments to equation (6) at the end of section 5.1 occurs. To find which case is realized, we analyse the temperature dependence of the resistivity in the magnetic field. The localization radius of small polarons in the PM phase was predicted to vary in the field according to the law [26]

$$\alpha(B) = \alpha(0)(1 + b_1B^2), \tag{7}$$

where $b_1 \sim \chi(T)$. If $b_1B^2 \ll 1$, it follows from equations (5)–(7) that

$$T_0(B) = T_0(0)(1 - b_2B^2), \tag{8}$$

where $b_2 = b_1T_{0SE}(0)\{T_0(0) - [T_0(0)/T]^{1/2}\gamma/(2k)\}^{-1}$ until γ is independent of B. This gives

$$\gamma(T) = 2\frac{b_1/b_2 - 1}{2b_1/b_2 - 1}k\sqrt{T_0(0)T}. \tag{9}$$

Near T_v, which is well above T_C, the temperature dependence of χ can be neglected [14]. Therefore, in the temperature intervals in the vicinity to T_v the dependences of T_0 and A on B can be found from linear fits of the plots of $\ln(\rho/T^{9/2})$ versus $T^{-1/2}$ in the field. The dependence of $\alpha(B)/\alpha(0)$ can be evaluated with equation (4). As can be seen from figure 8 the plots of $\alpha(B)/\alpha(0)$ versus B^2 and $T_0(B)/T_0(0)$ versus B^2 are linear functions up to $B = 10$ T for S100, S125 and at least up to $B = 8$ T for S154. The values of the ratio of $b_1/b_2 = 1.24 \pm 0.04$, 1.26 ± 0.06 and 1.28 ± 0.05 for S100, S125 and S154, respectively, are found to lie above unity with the deviation from unity being much larger than the error. This means the existence of a non-zero rigid gap near T_v depending on T as $\gamma(T) \approx \gamma(T_v)(T/T_v)^{1/2}$ with the values of $\gamma(T_v)$ given in table 3.

To evaluate the localization radius, we use for the DOS outside the Coulomb gap the expression $g_0 \approx N_0\phi\sigma\eta/W$ [27], where $N_0 = 1.74 \times 10^{22}$ cm^{-3} is the concentration of the Mn sites, W is the width of the band of the localized states, $\eta \approx c$ is the concentration of the holes or the probability that the Mn site receiving the hopping electron is unoccupied, $\phi \approx 0.5$ is a geometric factor and $\sigma \approx 1 - c$ is the probability that an unoccupied Mn site can actually accept an electron [27]. The values of W can be calculated using the equation $kT_C \approx 0.05Wc(1-c)$ [26] with T_C found from the magnetization measurements [14]. Then κ is evaluated with equation $g_0 = (3/\pi)(\kappa^3/e^6)[\Delta - \gamma(T_v)]^2$ [8], yielding $\kappa \approx 3.5$, and finally α is found using equations (5) and (6) (see table 3).

5.3. Discussion

The temperature dependence of the pre-exponent $\rho_0(T) = AT^m$ in equation (2) given by $m = 9/2$ for $\Gamma \gg 1$ in the investigated samples means that the fluctuating short-range

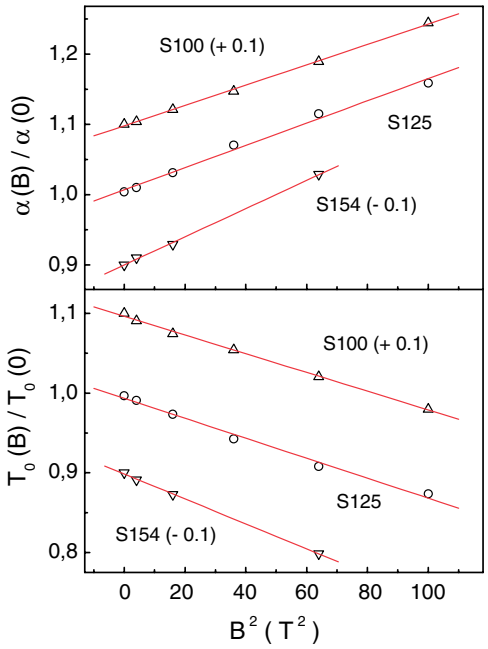

Figure 8. The dependences of $\alpha(B)/\alpha(0)$ on B^2 (upper panel) and $T_0(B)/T_0(0)$ on B^2 (lower panel). For convenience the plots for S100 and S154 are shifted along the y-axis by ± 0.1 units. The solid lines are linear fits.

potential, connected to the lattice disorder, is not important for the carrier localization in $LaMnO_{3+\delta}$. This is an indication of the rather homogeneous distribution of the holes, as mentioned above. A similar situation was observed in $La_{1-x}Ca_xMnO_3$ with $x = 0.3$. Only in the $La_{1-x}Ca_xMn_{1-y}Fe_yO_3$ samples with y between 0.03 and 0.09 the dependence $\rho_0 \sim T^{5/2}$ was found, indicating an additional short-range lattice disorder induced by doping with Fe [8]. Using the values of α and T_0 obtained in this work it can be shown directly that the condition of $\Gamma \gg 1$ is satisfied in all the investigated $LaMnO_{3+\delta}$ samples.

The values of the width of the soft gap, Δ, in $LaMnO_{3+\delta}$ are close to those in $La_{0.8}Ca_{0.2}MnO_3$ [9] and $La_{0.7}Ca_{0.3}Mn_{1-y}Fe_yO_3$ [8]. On the other hand, Δ should be comparable with the energy of the Coulomb interaction $U \approx e^2/(\kappa R)$ where $R = 2(4\pi N_h/3)^{-1/3}$ is the mean distance between the holes and $N_h = cN_0 = 2\delta N_0$ is the concentration of the holes [10]. The values of $U \approx 0.51, 0.55$ and 0.59 eV for S100, S125 and S154 are found to be similar to those of Δ, increasing with δ in agreement with the corresponding increase of Δ in table 3.

The value of $\kappa \approx 3.5$ is smaller than the static dielectric constant, $\kappa_0 = 16$ [28], because the average distance between the holes in $LaMnO_{3+\delta}$ is about the lattice parameter. This does not permit to perform a macroscopic averaging of the Coulomb interactions of the holes, so that κ does not represent a true dielectric constant, but an effective parameter lying between 1 and κ_0, corresponding to interactions in vacuum and in the medium. A similar value of $\kappa \approx 3.4$ characterizes the Coulomb interaction of the localized carriers in $La_{1-x}Ca_xMn_{1-y}Fe_yO_3$ [8].

The values of α are consistent with small polaron formation [11]. In addition, they decrease with δ as may be expected from the corresponding increase of the degree of the localization due to progressive distortions of the perovskite structure. This behaviour agrees with the evolution of the magnetic properties of $LaMnO_{3+\delta}$ [14], in particular with the decrease of T_C

when δ is increased above 0.1 (see also the inset to figure 5). As can be seen from the bottom panel of figure 7, A is a linear function of $\alpha^{11}T_0^{7/2}$, satisfying equation (4) and supporting the dependence of $\alpha(\delta)$ in table 3.

Finally, the values of $\gamma(T_v)$ are similar to those in $La_{0.8}Ca_{0.2}MnO_3$ [9] and $La_{0.7}Ca_{0.3}Mn_{1-y}Fe_yO_3$ [8]. On the other hand, they are comparable with the activation energy of the adiabatic nearest-neighbour hopping of small polarons $E_0 \approx E_b/2$, where E_b is the polaron binding energy [11]. Therefore, the origin of the rigid gap in the manganite perovskites is attributable to the polaron formation. The point is that to hop from one site to another the carrier should annihilate the polarization on the initial site and create it on the final site. This requires a minimum energy available for the hopping leading to appearance of the rigid gap in the DOS around μ if the local lattice distortions are the main reason for localization of the carrier, whereas that from the lattice disorder is much smaller. Namely, this case we have in $LaMnO_{3+\delta}$, where the lattice distortions are increased with growing δ and the lattice disorder is reduced, can explain the enhancement of γ when δ is increased (table 3). It is interesting to note that in $La_{0.7}Ca_{0.3}Mn_{1-y}Fe_yO_3$ we have quite the opposite situation: the distortions of the lattice due to Fe ions are small because when doping $La_{1-x}Ca_xMnO_3$ with Fe the Mn^{4+} ions are substituted with Fe^{3+}, having the same ionic radii [29]. Still the disorder is increased [8, 24, 30], leading to a finite distribution of the carrier potential energy and as a result to diminution of the rigid gap by the value of the width of this distribution when y is increased [8].

6. Conclusions

X-ray powder diffraction measurements and iodometric titration establish that $LaMnO_{3+\delta}$ prepared by the solid-state reaction exists for $\delta = 0.00$ in orthorhombic, for $\delta = 0.065$–0.112 in cubic with small rhombohedral distortions and for $\delta = 0.125$–0.154 in rhombohedral modifications. These structural modifications are confirmed by Raman spectroscopy showing a change of an ordered structure in S000 to a disordered one in S065 and in S154. The splitting observed on x-ray and Raman spectra is consistent with a lower symmetry of S154. The broadening of the maxima is assigned to a change in the Mn–O bonding.

The resistivity of $LaMnO_{3+\delta}$ is decreased when δ is increased and exhibits an activated behaviour in the whole range of temperatures between ~20 and 350 K, without showing a metal–insulator transition up to $c \approx 0.3$. The magnetoresistance has features common with $La_{1-x}Ca_xMnO_3$ (the CMR effect near T_C) and those not observed in $La_{1-x}Ca_xMnO_3$, like the non-monotonic dependence of CMR on δ and complex temperature dependence of $\Delta\rho/\rho_0$ below T_C.

The resistivity of $LaMnO_{3+\delta}$ in the PM phase between T_C and $T_v \sim 250$–270 K is determined by a complex energy dependence of the density of the localized states near the Fermi level, comprising the soft Coulomb gap and the rigid gap, both increasing with growing δ. The increase of the width of the Coulomb gap (Δ) is explained by increase of the hole concentration $c = 2\delta$. The enhancement of the width of the rigid gap (γ), which is connected to small-polaron formation, is interpreted by progressive lattice distortions in conditions of reduced lattice disorder. The dependence of the localization radius α on δ is observed and explained by increasing degree of the localization of the holes due to lattice distortions, enhancing when δ is increased.

Acknowledgments

This work is supported by the Wihuri Foundation, Finland, and by INTAS (Project No. INTAS 00-00728).

References

[1] Von Helmolt R, Wecker J, Holzapfel B, Schulz L and Sammer K 1993 *Phys. Rev. Lett.* **71** 2331
Schiffer P, Ramirez A P, Bao W and Cheong S-W 1995 *Phys. Rev. Lett.* **75** 3336
[2] Ramirez A P 1997 *J. Phys.: Condens. Matter* **9** 8171
[3] Coey J M D, Viret M and von Molnar S 1999 *Adv. Phys.* **48** 167
[4] Laiho R, Lisunov K G, Lähderanta E, Petrenko P A, Salminen J, Stamov V N and Zakhvalinskii V S 2000 *J. Phys.: Condens. Matter* **12** 5751
[5] Laiho R, Lähderanta E, Salminen J, Lisunov K G and Zakhvalinskii V S 2001 *Phys. Rev.* B **63** 094405
[6] Snyder G J, Hiskes R, DiCarolis S, Beasley M R and Geballe T H 1996 *Phys. Rev.* B **53** 14434
[7] Worledge D C, Snyder G J, Beasley M R and Geballe T H 1996 *J. Appl. Phys.* **80** 5158
[8] Laiho R, Lisunov K G, Lähderanta E, Petrenko P A, Salminen J, Shakhov M A, Safontchik M O, Stamov V S, Shubnikov M V and Zakhvalinskii V S 2002 *J. Phys.: Condens. Matter* **14** 8043
[9] Biswas A, Elizabeth S, Raychaudhuri A K and Bhat H L 1999 *Phys. Rev.* B **59** 5368
[10] Shklovskii B I and Efros A L 1984 *Electronic Properties of Doped Semiconductors* (Berlin: Springer)
[11] Mott N F and Davies E A 1979 *Electron Processes in Non-Crystalline Materials* (Oxford: Clarendon)
Mott N F 1990 *Metal–Insulator Transitions* (London: Taylor and Francis)
[12] Laiho R, Lisunov K G, Lähderanta E, Stamov V N, Zakhvalinskii V S, Kurbakov A I and Sokolov A E 2004 *J. Phys.: Condens. Matter* **16** 881
[13] Töpfer J and Goodenough J B 1997 *J. Solid State Chem.* **130** 117
[14] Laiho R, Lisunov K G, Lähderanta E, Petrenko P A, Salminen J, Stamov V N, Stepanov Yu P and Zakhvalinskii V S 2004 *J. Phys. Chem. Solids* **64** 2313
[15] Laiho R, Lisunov K G, Lähderanta E, Petrenko P A, Stamov V N and Zakhvalinskii V S 2000 *J. Magn. Magn. Mater.* **213** 271
[16] Dabrowski B, Xiong X, Bukowski Z, Dybzinski R, Klamut P W, Siewenie J E, Chmaissem O, Shaffer J, Kimball C W, Jorgesen J D and Short S 1999 *Phys. Rev.* B **60** 7006
[17] Nowotny J and Recas M 1998 *J. Am. Ceram. Soc.* **81** 67
[18] Poulsen F W 2000 *Solid State Ion.* **129** 145
[19] Dediu V A, Lopez J, Matacotta F C, Nozar P, Ruani G, Zamboni R and Taliani C 1999 *Phys. Status Solidi* b **215** 625
[20] Iliev M N, Abrashev M V, Lee H-G, Popov V N, Sun Y Y, Thomsen C, Meng R L and Chu C W 1998 *Phys. Rev.* B **57** 5
[21] Huhtinen H, Laiho R, Lisunov K G, Stamov V N and Zakhvalinskii V S 2002 *J. Magn. Magn. Mater.* **238** 160
[22] Chechersky V, Nath A, Isaac I, Franck J P, Ghosh K, Ju H and Greene R L 1999 *Phys. Rev.* B **59** 497
Hennion M, Moussa F, Biotteau G, Rodriguez-Carvajal J, Piusard L and Revcolevschi A 1998 *Phys. Rev. Lett.* **81** 1957
[23] Huhtinen H, Laiho R, Lähderanta E, Salminen J, Lisunov K G and Zakhvalinskii V S 2002 *J. Appl. Phys.* **91** 7944
[24] Laiho R, Lähderanta E, Salminen J, Lisunov K G, Zakhvalinskii V S, Safontchik M O, Shakhov M A and Shubnikov M L 2002 *J. Appl. Phys.* **91** 7400
[25] Zheng R K, Zhu C F, Xie J Q and Li X G 2000 *Phys. Rev.* B **63** 024427
[26] Varma C M 1996 *Phys. Rev.* B **54** 7328
[27] Viret M, Ranno L and Coey J M D 1997 *Phys. Rev.* B **55** 8067
[28] Alexandrov A S and Bratkovsky A M 2000 *J. Appl. Phys.* **87** 5016
[29] Jonker G H 1954 *Physica* **20** 1118
Ahn K H, Wu X W, Liu K and Chien C L 1996 *Phys. Rev.* B **54** 15299
[30] Laiho R, Lisunov K G, Lähderanta E, Salminen J and Zakhvalinskii V S 2002 *J. Magn. Magn. Mater.* **250** 267